Assessment of dynamic soil-structure interaction effects for tall buildings: a 3D numerical approach

by Riccardo Scarfone[1], Marco Morigi[2] & Riccardo Conti[3]

[1]PhD Student, University of Glasgow, School of Engineering, Rankine Building, Oakfield Avenue, Glasgow (UK), G12 8LT
e-mail: Riccardo.Scarfone@glasgow.ac.uk

[2]PhD Student, DICII, Universita` di Roma Tor Vergata, Rome, Italy.
e-mail: marco.morigi@uniroma2.it

[3]Associate Professor, Niccolò Cusano University, Via Don Carlo Gnocchi, 3, 00166 Rome, Italy
e-mail: riccardo.conti@unicusano.it

Contact Author:
Mr. Riccardo Scarfone
University of Glasgow, School of Engineering
Rankine Building, Oakfield Avenue, Glasgow (UK), G12 8LT
e-mail: Riccardo.Scarfone@glasgow.ac.uk

6895 **words**
7 **tables**
16 **figures**

Abstract

Soil-structure interaction (SSI) phenomena are typically studied in the frequency-domain using the substructure approach, involving several simplifications. In this study, SSI effects for a 20-storey building are studied numerically performing time-domain 3D non-linear dynamic analyses, using an elastoplastic nonlinear constitutive model for the soil. Three foundation systems - a relatively shallow, a deeply embedded and a pile foundation - and two soil profiles are investigated and compared. Specifically, relative merits of site amplification, kinematic interaction and inertial interaction are isolated, and the role of foundation deformability and local stratigraphy is highlighted. To isolate such features, the results of the complete 3D models are compared with those provided by 3D numerical analyses of the sole building, of the foundation-soil systems and of the free-field soil deposit.

Numerical results show that, for tall buildings, an increase in foundation deformability leads to a decrease of the maximum base shear force (seismic demand), to a higher rigid rotation of the foundation, but not to appreciably higher displacements of the structure. Moreover, possible situations where a (decoupled) substructure approach can lead to a misinterpretation of SSI phenomena are highlighted, as in the case of deep foundations crossing very soft soil layers.

In addition, the use of embedded pile elements was proven to be an effective strategy in reducing the computational cost when performing complex 3D simulations of dynamic SSI problems.

Keywords:
Dynamic soil-foundation-structure interaction
3D Finite difference model
Direct approach
Soft soil layer
Filtering effect
Foundation rocking

INTRODUCTION

The role played by the soil-structure interaction (SSI) on the seismic response of structures has been widely investigated in the literature [1]. On the one hand, dissipative mechanisms acting in the foundation-soil system, in the form of both hysteretic and radiation damping, always reduce the seismic demand of the structure with respect to its fixed-base counterpart. On the other hand, the increase in the overall system deformability can either reduce or amplify the inertia forces on the structure, depending also on the frequency content of the input earthquake [2].

When looking at the seismic response of slender structures, the most important factor in lengthening their fundamental period is the rotation of the foundation [3], which can even lead to a partial seismic isolation of the above structure if the moment capacity of the foundation is attained and plastic mechanisms occur in the foundation-soil system [4]. Leaving apart rocking isolation, which has a minor relevance in the seismic performance of tall buildings, Carbonari *et al.* [5] and Hokmabadi *et al.* [6] have shown that foundation rocking usually reduces the base shear (structural demand) in frame and coupled wall–frame systems, but can be responsible for additional interstorey drift. A more general result is provided by Bárcena & Esteva [7] and Zhang & Tang [8], showing that the effect of foundation rocking on the structural drift (ductility demand) depends essentially on the structure/input frequency ratio or, in other words, on the location of the natural period of the system on the elastic spectrum of the input earthquake.

The dynamic SSI problem and, more in general, the effects of soil deformability on the seismic behaviour of structures, are traditionally addressed using the so-called substructure approach, in which the relative contributions of site amplification, kinematic interaction (between the foundation and the soil) and inertial interaction (between the structure and the foundation-soil system) are investigated separately [1]. This decoupled approach, which strictly holds under the assumption of system linearity, involves many simplifications, most of them regarding the representation of the soil-foundation system. As a matter of fact, the kinematic interaction problem is described by means of real-valued, frequency-dependent functions relating the motion of the foundation to the free-field one

[9,10], while the inertial interaction problem is typically solved by reducing the soil-foundation system to a set of complex-valued, frequency-dependent impedance functions, representing its stiffness and dissipative properties [11]. Both set of functions are derived assuming a viscoelastic soil behaviour and, therefore, must be referred to an average value of the shear strain mobilised within the foundation-soil system during the earthquake.

Given its inherent simplifications, the substructure approach cannot describe adequately dynamic SSI if relevant nonlinearities are expected in the mechanical response of the soil. In this case, a direct approach must be used, where the whole structure-foundation-soil system is modelled and its dynamic response is analysed in the time domain. Within this context, more advanced constitutive models can be introduced, indeed, to take into account properly soil nonlinearity and plasticity.

A direct approach always requires a significant computational effort, related not only to an appropriate description of the constitutive soil response, but also to the often complex geometry of the structure to be modelled and to a proper representation of the foundation elements, especially in the case of piles, and of their mechanical interaction with the surrounding soil. As a result, nonlinear dynamic analyses are typically carried out in 2D plane strain conditions [12-14], while more realistic 3D models of the whole structure-foundation-soil system are rarely implemented in the literature [6,15-18].

This paper presents a 3D numerical study on the effects of SSI on the seismic response of a tall building with a wall-frame structural system. Three different foundation systems are taken into account – including a relatively shallow, a deeply embedded and a pile foundation – in order to highlight the role of foundation deformability and rocking on the dynamic response of the building. Along the same line, two different soil profiles are investigated, allowing to identify possible local stratigraphic effects on the behaviour of both the structure and the foundation.

Emphasis is given to the relative merits of local site amplification, kinematic interaction and inertial interaction on the overall structural response. In order to isolate such features, the results of

the complete 3D structure-foundation-soil models are systematically compared with those provided by 3D numerical analyses of the sole building (fixed-base structure), of the foundation-soil systems (kinematic interaction) and of the free-field soil deposit. This comparison allows to highlight also possible situations in which a decoupled approach can lead to a misinterpretation of dynamic SSI phenomena, as in the case of deep foundations crossing very soft shallow soil layers.

Nonlinear dynamic analyses were carried out in the time domain using the 3D finite difference code FLAC3D [19]. An elastoplastic hysteretic constitutive model was adopted for the soil, while a linear behaviour was assumed for the structural elements. Moreover, in order to improve the computational efficiency, embedded pile elements were introduced to model the pile foundation. While their performance under static loads is well established in the recent literature [20-23], their behaviour under dynamic conditions was verified in this work through *ad hoc* numerical simulations.

SYSTEM UNDER INVESTIGATION

This section provides the most relevant information on the system under investigation, comprising a 20-storey building, two subsoil models and three foundation systems. Moreover, details of the adopted seismic inputs are given in the following.

Geotechnical soil models

Two different geotechnical soil models were considered in this study, in order to highlight possible effects induced by local stratigraphic heterogeneities on the overall dynamic response of the soil-foundation-structure system.

The reference soil profile corresponds to a well characterised site in the eastern area of Napoli, Italy [24]. The corresponding stratigraphic profile (Model S1) is shown in Figure 1a, together with the assumed shear wave velocity profile, the latter obtained from the elaboration of Downhole and Crosshole test data. It consists of made ground (R), overlying volcanic ash (C) and pyroclastic silty sand (cohesionless pozzolana, Ps, and weakly cemented pozzolana, Pc), alternating with alluvial soils

(peat, T, and sand, S). A relatively rigid bedrock is assumed beyond a depth of 60 m. Specifically, the reference profile is characterised by the presence of a very soft peaty layer, with a thickness of 2 m, located at a depth of 10 m below ground level. Figure 1(c,d) shows the assumed modulus reduction and damping curves, obtained from the elaboration of Resonant Column tests and from literature data. Table 1 summarises all the relevant mechanical and physical properties for the soil layers.

The second geotechnical soil model (Model S2 in Figure 1b) differs from the first one only by the fact that the peat layer is missing and the volcanic ashes are assumed to extend down to the underlying sand layer. The comparison of the results obtained from subsoils S1 and S2 will highlight the role of the very soft peat layer in the dynamic SSI problem.

Building and foundation systems

A 20-storey high rise building, designed according to the Italian building code [25], is taken as reference, with a 30x20 m^2 rectangular plan and a total height H = 66 m above ground level. As shown in Figure 2, the building has a regular symmetric wall-frame structural system, where the steel columns and beams are coupled with reinforced-concrete (RC) shear walls through the floor slabs. Specifically, the seismic resistant system is composed by four RC shear walls, two oriented along each principal direction, and one RC core wall with a hollow rectangular cross section. The cross-section of the RC walls is constant along the height, while the steel columns do taper every three floors.

Three foundation systems are considered in this work (see Figure 3) in order to analyse the role of the foundation on the dynamic response of the building. The first foundation (F1 in Figure 3a,b) is the reference one. It was chosen with similarity with the actual foundation system typically adopted in the reference site [24].

Foundation F1 includes one 3m-thick basement floor beneath ground level, with a dense grid of RC diaphragm walls forming relatively stiff structural boxes, overlying a 1m-thick RC base slab, for a total embedment of 4 m. The foundation system is integrated by a 6×4 pile group of large diameter

(d = 2 m), with a length of 40 m and a regular spacing of 5 m (Figure 3a,b). The piles, designed essentially as settlement reducers for the subsoil profile S1, are rigidly connected with the base slab. Foundation F2 is a classical compensated foundation, with three basement floors beneath ground level 1overlying a 1m-thick RC base slab (Model F2 in Figure 3c). In this case, the total embedment depth of the foundation is D = 10 m. Model F3, instead, refers to a relatively shallow raft foundation, with only one floor below ground level and a total embedment depth of D = 4 m (Figure 3d). The latter is under-designed for the subsoil profile S1, where the soft peaty layer would cause excessive settlement of the building. For the case of subsoil S1, in fact, vertical settlements of 6.3 cm and 0.8 cm were computed under gravitational (static) loads, for foundation models F3 and F1, respectively. Nonetheless, as will be shown in the following sections, a direct comparison between the three models clarifies the influence of the foundation compliance on the dynamic response of the structure, as well as, some aspects related to the kinematic interaction between the foundation and the stratified soil deposit.

Seismic inputs

The input signals were selected to be compatible with the code-specified spectrum for the life-safety limit state, corresponding to an earthquake with a return period of 712 years. Specifically, the software Rexel [26] was used to select seven natural acceleration time histories from the European strong motion database, all recorded on rock outcrop. The accelerations were low-pass filtered at 10 Hz, base-line corrected using a standard polynomial detrending algorithm, and scaled to a maximum acceleration of 0.192 g. A cut-off frequency of 10 Hz was chosen to limit the computational time without affecting the significance of the results. Figure 4 shows the elastic response spectra (i.e. pseudo-spectral acceleration, *PSa*, against period, *T*) at 5% damping of the selected signals, while Table 2 summarises the corresponding ground motion parameters, *i.e.*: peak ground acceleration, *PGA*; peak ground velocity, *PGV*; peak ground displacement, *PGD*; dominant frequency, f_d; mean frequency, f_m; Arias intensity, I_a; and strong motion duration, $T_{5\text{-}95}$.

NUMERICAL MODEL

Four numerical models were analysed, with reference to the idealised case study presented in the previous section, *i.e.*:

1) the fixed base structure, to identify the dynamic characteristics (natural frequencies and modal shapes) and the seismic response of the building without SSI effects;
2) the one-dimensional free-field soil deposit, to highlight the influence of the local stratigraphy on the characteristics of the surface ground motion;
3) the soil-foundation model, to isolate aspects concerning the sole kinematic interaction problem;
4) the complete soil-foundation-structure model, to investigate the dynamic response of the whole system with a direct approach;

As an example, Figure 5 shows some details of the mesh and of the structural elements used to model the complete soil-foundation-structure system, for the three foundation typologies (F1, F2 and F3) and the subsoil profile S1. The mesh, comprising 22200 elements, has plan dimensions of 90×60 m^2, chosen to minimize boundary effects on the building response during both the static and the dynamic stage, and a total depth of 62 m. Following Lysmer & Kuhlemeyer [27], the size of the elements was chosen in order to describe correctly the minimum wavelength of the applied signals. Standard boundary conditions were applied during the initial (static) stage, that is zero horizontal displacements along the lateral boundaries and fixed nodes at the base of the grid.

During the subsequent (dynamic) stage, the seismic inputs were applied to the bottom nodes of the mesh, along the x-x horizontal direction. Neither the vertical component of the input motion, nor its component along the orthogonal y-y horizontal direction, were considered in this study. In order to take into account the finite stiffness of the underlying bedrock, and to reproduce the upward propagation of shear waves within a semi-infinite domain, a standard deconvolution procedure was carried out [28]. According to this procedure: (i) the outcrop input accelerations were halved to

compute the corresponding upward-propagating wave motion; (ii) the accelerations were integrated to obtain velocities; (iii) the velocity was converted to a shear stress time history and applied to the bottom nodes together with adsorbing viscous dashpots.

Free-field boundary conditions were applied along the lateral sides of the mesh, involving the coupling of the main grid with a one-dimensional free-field column through viscous dashpots, in order to absorb outward waves originating from the interior of the model.

A time increment of $\Delta t = 5 \cdot 10^{-5}$ s was adopted during the dynamic stage, to guarantee the stability of the explicit time integration scheme.

Effective stress analyses were carried out in drained conditions, assuming that the pore-pressure distribution is not affected by mechanical deformation. As a result, possible variations of pore water pressures due to deviatoric-volumetric strain coupling under cyclic loading are not taken into account.

The soil

The soil was modelled as an elastic-perfectly plastic material with a Mohr-Coulomb failure criterion and a standard non-associated flow rule, with angle of dilatancy $\psi = 0$. During the dynamic stage, non-linear and hysteretic behaviour was introduced for stress paths within the yield surface through a hysteretic model available in the library of FLAC3D, extending to general strain conditions the unloading-reloading Masing [29] rules. The constitutive soil model is completely defined by two elastic parameters (the small strain shear modulus, G_0, and the Poisson's ratio, v), two strength parameters (friction angle, φ', and cohesion, c') and three parameters controlling the shear modulus degradation curve (a, b and x_0), according to the equation:

$$\frac{G(\gamma)}{G_0} = \frac{a}{1+exp[-(\gamma - x_0)/b]} \quad (1)$$

Table 3 summarizes the constitutive parameters adopted for each soil layer, while the corresponding $G/G_0(\gamma)$ and $D(\gamma)$ curves are shown in Figure 6. Other soil properties (ρ and V_S) coincide with those assumed in the geotechnical subsoil profile (see Table 1). Finally, a small

Rayleigh viscous damping (D = 0.5% at f = 2.0 Hz) was assigned to the soil elements in order to remove the high-frequency noise deriving from the numerical integration, but not otherwise affecting the results of the analyses.

The structure

The building was modelled using standard 1D beam elements for the columns and 2D shell elements for the floor slabs and the vertical shear walls, assuming a linear elastic isotropic behaviour for all the structural elements.

Beams are straight finite elements of uniform bisymmetrical cross-sectional properties and with two nodes, each one characterised by six degrees of freedom (3 translational and 3 rotational). According to the reference building model, seven orders of steel columns were defined, each one composed by 40 beam elements, characterised by the same physical and mechanical properties (ρ = 7.91 t/m^3, E = 2.1×10^8 kPa and v = 0.3) but with different sections. Table 4 summarises the geometrical properties of the beams, *i.e.*: the cross section area, A_s; the polar moment of inertia, J_t; and the moments of inertia with respect to the x and y axes, I_x and I_y.

Shell elements are three-node, flat finite elements with six degrees of freedom per node. Their numerical formulation, given by a superposition of membrane and bending response, is suitable for modelling thin-shell structures in which the displacements caused by transverse-shearing deformations can be neglected. Table 5 summarises the physical and mechanical parameters of the shell elements, together with their thickness, t_s, which defines completely the geometry of the cross section area.

A non-viscous damping formulation was used for the structural elements, called local damping in FLAC3D terminology, which operates by adding or subtracting mass from a structural node at certain times during a cycle of oscillation, thus resulting in a frequency-independent energy dissipation [19, 30, 31]. The adopted damping ratio was D = 5 %.

The embedded foundation

Both the 1 m-thick base slab and the dense structural grid of RC walls composing the underground floors were modelled with linear elastic solid elements (see Figure 5). Specifically, in order to simplify the numerical model, the stiff basement was reduced to an equivalent full solid with the same total mass and an impedance ratio of about 10 with respect to the surrounding soil elements, such as to guarantee a virtually rigid behaviour of the embedded foundation. Table 6 reports the physical and mechanical parameters assumed for these elements. Perfect bond was assumed between the embedded foundation and the surrounding soil (*i.e.* no interface elements were used), thus neglecting any possible relative displacement between the structure and the soil, in the form of uplifting or sliding. This assumption is consistent with the structural system under investigation, corresponding to which no relative displacements are expected to occur under the applied input earthquakes. Moreover, the assumption was verified *a posteriori* in all the analyses, by making sure that the stress state at the interface between the bottom of the foundation and the soil is entirely in compression. With this regard, it was observed that the interaction between the soil and the external basement walls resulted crucial in the prevention of uplifting.

Pile elements

Piles were modelled using embedded pile elements, composed by two-node beam elements with six degrees of freedom per node, interacting with the surrounding soil continuum elements through normal and shear elastic-perfectly plastic interfaces. Specifically, each pile was modelled with 40 identical beam elements of 1 m-length, assuming a linear elastic behaviour with typical RC physical and mechanical properties (ρ = 2.5 t/m^3, E = 3.3×10^7 kN/m^2, ν = 0.15), while pure frictional interfaces where adopted along the pile length, in direction both perpendicular and parallel to the pile axis. These interfaces, which aim at reproducing the 3D load transfer mechanism occurring between the pile and the adjacent soil under both vertical and horizontal loading, are defined by their shear and normal stiffness, k_s and k_n, the friction angles φ_s and φ_n, and the exposed perimeter of the pile, p.

More in detail, the maximum shear force ($f_{s,max}$) and normal force ($f_{n,max}$), for unit length of embedded pile, are related to the average effective confining stress, σ'^{avg}_n, through:

$$f_{s,max} = \sigma'^{avg}_n (tan\ tan\ \phi_s)\ p \quad (2)$$

$$f_{n,max} = \sigma'^{avg}_n \phi_n)\ p \quad (3)$$

As a result, φ_s can be taken as being equal to the soil friction angle ($\varphi_s = \varphi'$), at least in the case of bored piles. On the other hand, φ_n can be estimated by equating $f_{n,max}$ to the drained ultimate lateral soil resistance, p_u. Specifically, according to the Broms' theory, $p_u = 3K_p \cdot \gamma \cdot d \cdot z$, where K_p is the passive earth pressure coefficient, d is the pile diameter and z is the reference depth, and then:

$$\phi_n = \left(\frac{3K_p}{\pi K_0}\right) \quad (4)$$

where K_0 is the earth pressure coefficient at-rest. Table 7 summarizes the values adopted for the interface parameters, depending on the mechanical properties of the interacting soil layers.

In order to model the end bearing capacity of the piles, an elastoplastic spring was applied at the tip of each pile, with stiffness $k_p = 1 \times 10^8$ kN/m^3 and compressional yield strength $y_c = 25446$ kN, which corresponds to the estimated theoretical value of the end bearing capacity of the single pile.

The computational efficiency and the ability of embedded pile elements to reproduce accurately the interaction between the pile and the surrounding soil under vertical and horizontal static loads was recently verified by many Authors [20-23]. To investigate their behaviour under dynamic loading, a simple numerical test was carried out, in which a single pile (diameter, $d_p = 1$ m; length, $L_p = 25$ m; $\rho_p = 2.5$ t/m^3; $E_p = 3 \times 10^7$ kPa; $\nu_p = 0.2$), fixed at the top, is immersed in a homogeneous linear viscoelastic soil deposit ($E_s/E_p = 1000$; $\rho_s/\rho_p = 0.7$; $\nu_s = 0.3$; $D_s = 5\%$). The mesh has plan dimensions of 21×21 m^2 and a total depth of 30 m, with a constant discretization of 1m along the vertical direction. Free-field boundaries were applied along the vertical sides of the mesh, while a rigid bedrock condition was imposed at the base. Following the embedded pile approach, the pile was modelled with 25 identical beam elements, connected to the soil continuum elements through linear elastic springs. Both the frequency-dependent kinematic interaction factor $I_u = U_p/U_{ff0}$, where U_p is

the horizontal displacement of the pile head and U_{ff0} is the surface free-field motion, and the translational, K_H, and rocking, K_θ, complex impedances of the pile were computed. To this end, a constant amplitude sinusoidal sweep input was applied, in the form of: (i) a horizontal displacement time history applied at the base of the mesh, to compute I_u; (ii) a horizontal force applied at the top of the pile, when computing K_H; and (iii) a moment applied, again, at the pile head, to compute K_θ. A FFT algorithm was used to switch from time to frequency domain.

Figure 7 compares the numerical FDM results with solutions provided by more rigorous approaches. Specifically, $|I_u|$ values are compared with other analytical [32] and numerical [33] results available in the literature (Figure 7a), while the impedance functions are validated against numerical results obtained with the FEM code ANSYS, where both the pile and the soil are modelled using solid continuum finite elements (Figure 7b,c). The comparison shows a very good agreement, thus confirming the capability of the embedded pile strategy to model also the dynamic response of piles.

DISCUSSION OF RESULTS

The main results of the numerical 3D study are presented in the following sections. Specifically, frequency-dependent transfer functions will be also used to provide a deeper insight into the dynamic response of the nonlinear soil-foundation-structure system under the applied earthquakes. To this aim, the smoothing procedure described in Conti & Viggiani [34] was adopted to remove the noise-dominated frequencies from the data interpretation.

Dynamic identification of the structure

The dynamic identification of the fixed-base structure along the x-x direction, that is the computation of its natural frequencies and the corresponding modal shapes, was carried out in the time domain by analysing the dynamic response of the 3D fixed-base model under both free and forced vibrations. In the first case, a pulse wavelet input signal was applied at the base of the structure, while a constant amplitude sinusoidal sweep was used in the second case, defined in terms of a horizontal displacement

time history, with a duration of 110 s and a frequency increasing linearly with time from 0.05 to 12 Hz.

Figure 8 shows (a) the acceleration and (b) the displacement time histories computed at different heights along the 3D model during its free and forced vibrations, respectively, while Figures 8(c,d) show the corresponding Fourier amplitude spectra, where the first three natural frequencies of the fixed-base model (f_1 = 0.75 Hz, f_2 = 3.90 Hz and f_3 = 9.50 Hz) can be clearly recognised. The normalised modal shapes of the structure were evaluated from the horizontal displacement distribution computed at time instants t_1, t_2 and t_3 during the forced vibrations, corresponding to which local resonance is attained in the model (Figure 8e). The computed modal shapes are in very good agreement with those provided by a modal analysis carried out with the FEM code SAP2000 [35] on an identical 3D model of the fixed-base structure. The latter allowed to compute also the corresponding modal participating mass ratios (M_1 = 63.5%, M_2 = 20.0%, M_3 = 6.8%), indicating that the dynamic response of the fixed-base model is dominated by its first mode.

Free-field seismic response analyses

The main results of the free-field site response analyses are summarised in Figure 9 for the subsoil models S1 and S2. Specifically, Figure 9 shows the profiles of (a, e) maximum acceleration, a_{max}, and (b, f) maximum shear strain, γ_{max}, mobilised within the soil deposit, together with (c, g) the frequency dependent surface-to-bedrock amplification functions of the soil deposit, $|F|=|U_{ff0}/U_{bed}|$, and (d, h) the elastic response spectra at surface.

As far as the subsoil model S1 is concerned, a concentration of shear strains is observed in the peat layer, leading locally to an abrupt reduction of the maximum accelerations (Figure 9a,b). As suggested by Bilotta *et al*. [24], this effect is related to the presence of the soft peaty layer, which essentially behaves as a natural damper for the high-frequency components of the upward propagating seismic waves. As a matter of fact, the maximum accelerations in the shallower strata are not damped in model S2, where the peat layer is missing.

A deeper understanding of the role played by the local stratigraphy is given by the computed amplification functions (Figure 9c,g), showing that the presence of the peaty layer tends to attenuate the high-frequency components (f > 3 Hz) of the input signals, but inducing major amplifications in the small-frequency range of (f = 0.7-2 Hz), where the first two natural frequencies of the soil deposit lie. On the one hand, in fact, the filtering capability of a very soft soil layer is activated only when its thickness exceeds a portion of the travelling wavelength [36], *i.e*. seismic isolation is typically confined in the high-frequency range. On the other hand, the presence of the soft layer increases the overall deformability of the soil deposit, thus increasing possible amplifications in the small-frequency range.

The same conclusions can be inferred from the elastic response spectra computed at surface (Figure 9d,h), showing that, in model S1, spectral ordinates are reduced with respect to the bedrock ones in the low-period range (T < 0.3 s), due to the filtering action of the peat layer, while amplification phenomena are more pronounced at higher periods (T = 0.7-2 s). As a result, taking into consideration that the dominant period of the fixed-base structure is T_1 = 1.33 s, corresponding to which the average spectral acceleration is equal to 0.35 g for subsoil S1 (Figure 9d) and 0.29 g for subsoil S2 (Figure 9h), the presence of the soft peat layer is expected to increase the seismic demand of the building, in spite of the reduction of maximum accelerations at surface.

Kinematic interaction

As a result of the kinematic interaction between the foundation and the supporting soil, the horizontal displacement of the base slab is typically reduced with respect to the free-field motion, but a rotational component can appear, depending on the geometry of the foundation. This filtering effect, essentially related to the inability of the foundation elements to accommodate soil displacements, can be quantified by two dimensionless factors, I_u and I_θ, which are frequency-dependent transfer functions relating the harmonic steady-state motion of the foundation to the amplitude of the free-field surface motion [37].

In this work, the kinematic interaction problem was investigated with reference to the 3D numerical model of the sole foundation-soil system, by focusing only on the horizontal component of the foundation motion, as the geometry of the three footings makes the corresponding kinematic rotation indeed negligible.

Figure 10 shows, for one of the applied earthquakes (EQ2), the numerical values of $|I_u|=|U_{FIM}/U_{ff0}|$, computed as the ratio between the horizontal displacement atop foundation (U_{FIM}) and at the free-field surface (U_{ff0}). The analytical expressions of $|I_u|$, obtained for a homogeneous isotropic viscoelastic soil deposit, are also plotted for comparison. In particular, the simplified formula proposed by Di Laora & de Sanctis [9] was used for the pile foundation F1, whereas the one proposed by Conti *et al.* [10] was used for the compensated foundations F2 and F3. The soil properties (i.e. mass density ρ_S, shear wave velocity V_S and Young modulus E_S) were computed as a weighted average over a length of $10 \cdot d$ (foundation F1), where d is the pile diameter, and over the embedment depth of the foundation (F2 and F3). Moreover, in order to take into account soil nonlinearity, mobilised values of V_S and E_S were considered, corresponding to the maximum shear strain computed in free-field conditions.

As far as the subsoil model S2 is concerned, numerical values of $|I_u|$ are consistent with the analytical solutions for embedded and pile foundations, characterized by an increase of their filtering capacity with increasing frequency and embedment depth [10,38].

A completely different behaviour is observed in the case of subsoil S1 (Figure 10a), for both the F1 and F2 foundation models, where $|I_u|$ values even larger than one are attained for frequencies between 3 Hz and 7 Hz, indicating that the foundation motion is amplified with respect to the free-field one in this frequency range. Also, in this case numerical and theoretical values of $|I_u|$ are significantly different from each other. This result stems from the fact that the high-frequency attenuation induced, in free-field conditions, by the shallow peaty layer is inhibited when the latter is crossed by the foundation, as in the case of the pile (F1) and, to a lesser extent, the deep embedded (F2) foundation model. In this condition, in fact, the wave motion is partly transferred to the top of

the foundation by the stiffer structural elements, without undergoing further deamplification at high-frequencies due to the presence of the very soft soil layer.

Kinematic effects are summarised in Figure 11, showing the mean values, among all the seven applied earthquakes, of the 5% damping elastic response spectra of the foundation motions, for subsoils S1 (a) and S2 (b). For comparison, also the mean values of the free-field elastic response spectra are reported. In both subsoil models, foundation F3 provides a limited reduction of the spectral ordinates, with respect to the free-field case, due to its short embedment depth. As far as foundations F1 and F2 are concerned, spectral accelerations are always lower than the free-field ones in the case of subsoil S2, with the filtering effect increasing for lower periods (Figure 11b). This result is less evident for the subsoil S1 (Figure 11a), where the pile foundation provides spectral accelerations even larger than the free-field ones for spectral periods lower than 0.3 s.

As shown in Figure 11, the dominant period of the building, T_1, is located in a period range where filtering effects are always negligible, thus indicating that the dynamic response of the whole structure-foundation-soil system would be hardly affected by kinematic effects in this case. Moreover, since T_1 is situated on the descending branch of the elastic response spectrum, any increase in the system deformability due to SSI effects would imply a consequent reduction of the inertia forces on the structure.

Full dynamic interaction

In order to quantify SSI effects, the seismic response of the complete structure-foundation-soil system can be compared with its fixed-base counterpart, where the 3D model of the sole building is subjected to the free-field motion applied at its base.

Figure 12 shows the frequency dependent transfer functions, $|F|=|U_{STR}/U_{ff0}|$, between the horizontal displacement of the roof (U_{STR}) and the free-field surface motion (U_{ff0}). Black lines refer to the fixed-base model, while coloured curves correspond to the 3D models of the complete structure-foundation-soil system. As expected, the nonlinear behaviour of the supporting soil makes

the SSI effects strongly dependent on the applied input earthquake. However, as a general trend, dynamic SSI induces an increase of both the deformability ($f_{1,SSI} < f_{1,FIX}$) and damping ($D_{SSI} > D_{FIX}$) of the system, the latter being inversely proportional to the maximum of the U_{STR}/U_{ff0} curves. Moreover, these effects are more pronounced for the shallow foundation, F3, and in the case of the subsoil model S1, due to the softer response of the soil-foundation system.

Figure 13 shows a comparison between the fixed-base model and the complete structure-foundation-soil systems, in terms of: (a, c) maximum total shear force at the base of the seismic resistant shear walls (V), and (b, d) maximum relative displacement of the building (u_{rel}), computed between the roof and the base (z = 0 m). The latter quantity, which takes into account both the rigid rotation of the foundation and the structural deformation, is of practical interest in the design of seismic gaps between adjacent structures [5].

Looking at the response of the fixed-base structure, and comparing the numerical results obtained for the two subsoil models, the presence of the peaty layer clearly increases the seismic demand of the structure, in terms of both V and u_{rel}, as was anticipated based on the results of the free-field analyses. When taking into consideration the whole system, as expected, SSI reduces the inertia forces transmitted to the building and, hence, the maximum shear force in the structural members, which is reduced by an average amount of 36% and 61% in the case of the F1 and F3 foundation model, respectively (subsoil S1). However, the increased overall deformability of the system does not result in an increase of the maximum relative displacement of the structure.

The last observation is clarified by inspection of Figure 14, showing, as an example, the maximum deformed shape of the structure (a), the maximum drift ratio (b) and the residual seismically-induced foundation settlements (c), computed under the earthquake EQ7 (subsoil model S2). As expected, the inertial interaction between the structure and the underlying foundation-soil system induces rocking in the foundation and, in turn, increases the rigid displacement of the structure. This effect is more evident for the shallower and more compliant F3 foundation. On the other hand, the reduction of the inertia forces transmitted to the structure, due to the increased

deformability and damping of the system, significantly reduces its flexural deformation. These numerical results, strictly dependent on the relative importance of foundation rocking and structural deformation, are in agreement with the theoretical findings by Bárcena & Esteva [7] and Zhang & Tang [8], showing that SSI tends to reduce the ductility demand of the structure and the interstorey drift when the building is located in the descending branch of the elastic response spectrum. However, in spite of a reduction of the structural demand, the presence of a more compliant foundation system causes higher plastic deformations into the soil, which consequently lead to higher seismically-induced residual settlements and rotation, as shown in Figure 14(c). With reference to this point, it must be mentioned that more advanced constitutive soil models, including deviatoric-volumetric coupling, should be used for a more accurate computation of the volumetric plastic deformations into the soil and of the resulting structural settlements.

Dynamic response of piles

As far as foundation F1 is concerned, SSI effects on the dynamic response of the piles were assessed for both the subsoils S1 and S2, with reference to the earthquake EQ7, which caused the most critical loading condition in the piles. In particular, four different piles will be taken into consideration in the following discussion, namely p1, p2, p3 and p4 (see e.g. Figure 3b).

Figure 15 shows the loading path computed at the top section of the four piles during the full dynamic interaction analysis, *i.e.* in the complete soil-foundation-structure model. Specifically, the loading path is given in terms of the axial force N (positive sign means compression) and bending moment M. Given the polar symmetry of the circular section, the bending moment was calculated as:

$$M = \sqrt{{M_x}^2 + {M_y}^2} \qquad (5)$$

where M_x and M_y are the bending moments acting along the x-direction and y-direction, respectively. The structural failure domain of the piles is also plotted in Figure 15, corresponding to a circular reinforced concrete section with a diameter of 200 cm, reinforced with 100 steel bars with a diameter

of 26 mm. Piles p2 and p4, located at a higher distance from the centre of the foundation along the x-direction (direction of the input earthquake), are subjected to higher variations of the axial force *N*, whereas the bending moment *M* is less dependent on the location of the piles. The significant variation of *N* in the external piles is clearly related to the bending moment generated in the base slab by the inertia forces acting in the above structure. By comparing the results obtained for subsoils S1 and S2, it can be observed that the presence of the peat layer generates higher internal forces in the piles because, as previously discussed, the peat layer leads to a higher seismic demand for the foundation-structure system.

Bending moment in the piles emerges as a combination of two concurrent phenomena [39, 40]: the kinematic interaction with the soil during wave propagation, which can induce significant bending along the whole pile length, depending also on the constraint imposed to the pile head, and the inertial interaction with the superstructure, whose effects are typically confined close to a certain depth below the pile head [41]. In order to isolate kinematic from inertial effects, Figure 16 shows the envelope of the maximum bending moment along the piles, computed again during the earthquake EQ7. Specifically, dotted lines refer to the kinematic interaction analysis (KI), *i.e*. the sole soil-foundation model, while continuous lines refer to the full dynamic interaction analysis (DI). In these graphs, the depth is relative to the head of the piles, located 4 m below the ground surface (see *e.g.* Figure 3a). All the envelope profiles have a similar trend: the bending moment is maximum at the pile head; it decreases rapidly down to a depth of about 10 m, after which it remains approximately constant; then it reduces close to the tip, where it nullify. Moreover, KI and DI profiles show negligible differences, thus indicating that bending moment in the piles are mainly due to kinematic effects. This result holds also close to the pile head, where the fixed-head constraint imposed by the presence of the base slab (kinematic interaction effect) prevails over the inertia forces coming from the structure.

Finally, comparing the results obtained for the subsoils S1 and S2 (Figure 16), maximum bending moments in the piles are similar, starting from the tip and up to a depth of about 10 m. However, the presence of the peat layer leads to higher values of M_{max} in the upper part of the piles. This result is

consistent with the higher seismic demand caused by the presence of the peat layer, as discussed above. On the other hand, the stiffness contrast between the peat layer and the adjacent soil layers does not induce a further local increment of bending moment, probably due to the limited thickness of the peat layer.

CONCLUSIONS

Soil-structure interaction effects for a 20-storey building were assessed numerically performing non-linear dynamic analyses in the time domain using the 3D finite difference code FLAC3D. The effects of local site amplification, kinematic interaction and inertial interaction on the seismic response of the building were analysed in this study, also highlighting the role played by different foundation systems and by the presence of a very soft layer in the supporting soil.

The dynamic identification of the sole structure, in terms of natural vibration frequencies and modal shapes, was carried out in the time-domain analysing the dynamic response of the 3D fixed-base model under both free and forced vibrations. The results were in very good agreement with those obtained from a modal analysis performed with the FEM code SAP2000.

Numerical results showed that the presence of a soft soil layer has important effects on the dynamic soil-structure interaction. Looking at the free-field seismic response of the soil deposit, it was shown that the soft peaty layer reduces the high-frequency components (f > 3 Hz) and amplifies the low-frequency components (f= 0.7-2 Hz) of the upward propagating seismic waves. As a consequence, it behaves as a natural damper for the maximum accelerations computed at the soil surface. This effect, however, is significantly reduced if the soft layer is crossed by the foundation (as in the case of foundations F1 and F2 of this study) because the wave motion is partly transferred to the top of the foundation by the stiffer structural elements. This kinematic interaction effect would not have been captured using the traditional substructure approach, where the foundation input motion is computed directly from the free-field motion at surface. Moving to the dynamic interaction of the

whole structure-foundation-soil system, the presence of the soft peaty layer resulted in a higher seismic demand of the building.

Kinematic interaction effects were found to be of minor importance for tall buildings, characterized by low natural vibration frequencies. By contrast, inertial interaction effects were found to be much more significant. In particular, consideration of the full dynamic interaction led to an overall increase of damping and deformability of the soil-foundation-structure system, compared to the fixed-base structure. For such a slender building, whose first natural vibration period lies on the descending branch of the elastic response spectrum, an increase in deformability resulted in a lower seismic demand in terms of both total base shear force and maximum inter-storey drift. The use of a more compliant foundation system (e.g. F3), although it led to higher residual seismically-induced settlements, resulted in a lower seismic demand and higher rigid rotation of the foundation, but not in appreciably higher relative displacement of the building. It is important to highlight that these conclusions are based on the simplified assumption of a linear behaviour of the structure. Introducing non-linearity of the structure would probably cause a reduction in the seismic demand of both the fixed-base structure model and the complete soil-foundation-structure model.

Analysing the dynamic response of the piles, it was shown that maximum bending moments virtually depend on the kinematic interaction, whereas inertial effects are important for the dynamic axial forces exerted on the piles. The presence of the peat layer leads to a stronger increase of the maximum bending moment above the layer itself and close to the pile head.

Finally, the use of embedded pile elements was proven to be a reliable and effective strategy in reducing the computational cost of time-domain numerical analyses.

Acknowledgements

The work presented in this paper was developed with the financial support of the Italian Department of Civil Protection within the ReLUIS research project.

REFERENCES

[1] Roesset, J.M. (2013). “Soil Structure Interaction The Early Stages.” *Journal of Applied Science and Engineering*, 16(1), 1-8.

[2] Mylonakis, G., Gazetas, G. (2000). "Seismic soil-structure interaction: beneficial or detrimental?" *Journal of Earthquake Engineering*, 4(3), 277-301.

[3] Veletsos, A.S., Meek, J.W. (1974). “Dynamic behaviour of building foundation systems.” *Earthquake Engineering and Structural Dynamics*, 3, 121-138.

[4] Pecker A, Paolucci, R., Chatzigogos, C., Correia, A.A., Figini, R. (2014). “The role of non-linear dynamic soil-foundation interaction on the seismic response of structures.” *Bulletin of Earthquake Engineering*, 12(3), 1157-1176.

[5] Carbonari, S., Dezi, F., Leoni, G. (2012). “Nonlinear seismic behaviour of wall-frame dual systems accounting for soil–structure interaction.” *Earthquake Engineering and Structural Dynamics*, 41, 1651–1672.

[6] Hokmabadi, A.S., Fatahi, B., Samali, B. (2014). “Assessment of soil–pile–structure interaction influencing seismic response of mid-rise buildings sitting on floating pile foundations.” *Computers and Geotechnics*, 55, 172-186.

[7] Bárcena, A., Esteva, L. (2007). “Influence of dynamic soil–structure interaction on the nonlinear response and seismic reliability of multistorey systems.” *Earthquake Engineering and Structural Dynamics*, 36, 327–346.

[8] Zhang, J., Tang, Y., (2009). “Dimensional analysis of structures with translating and rocking foundations under near-fault ground motions.” *Soil Dynamics and Earthquake Engineering*, 29, 1330-1346.

[9] Di Laora, R., de Sanctis, L. (2013). “Piles-induced filtering effect on the Foundation Input Motion.” *Soil Dynamics and Earthquake Engineering*, 46, 52-63.

[10] Conti, R., Morigi, M., Rovithis, E., Theodoulidis, N., Karakostas, C. (2018). “Filtering action of embedded massive foundations: New analytical expressions and evidence from 2 instrumented buildings.” *Earthquake Engineering & Structural Dynamics*, 47(5), 1229-1249.

[11] Mylonakis, G., Nikolaou, S., Gazetas, G. (2006). "Footings under seismic loading: Analysis and design issues with emphasis on bridge foundations." *Soil Dynamics and Earthquake Engineering*, 26(9), 824-853.

[12] Menglin, L., Huaifeng, C.X., Yongmei Z. (2011). “Structure–soil–structure interaction: literature review.” *Soil Dynamics and Earthquake Engineering*, 31, 1724-1731.

[13] Celebi, E., Göktepe, F., Karahan, N. (2012). “Non-linear finite element analysis for prediction of seismic response of buildings considering soil-structure interaction.” *Natural Hazards and Earth System Sciences*, 12, 3495–3505.

[14] Hussien, M.N., Karray, M., Tobita, T., Iai, S. (2015). “Kinematic and inertial forces in pile foundations under seismic loading.” *Computers and Geotechnics*, 69, 166-181.

[15] Torabi, H., Rayhani, M.T. (2014). “Three dimensional Finite Element modeling of seismic soil–structure interaction in soft soil.” *Computers and Geotechnics*, 60, 9-19.

[16] Amorosi, A., Boldini, D., di Lernia, A. (2017). “Dynamic soil-structure interaction: A three-dimensional numerical approach and its application to the Lotung case study.” *Computers and Geotechnics*, 90, 34-55.

[17] de Silva, F., Pitilakis, D., Ceroni, F., Sica, S., Silvestri, F. (2018). “Experimental and numerical dynamic identification of a historic masonry bell tower accounting for different types of interaction.” *Soil Dynamics and Earthquake Engineering*, 109, 235-250.

[18] López Jiménez, G.A., Dias, D., Jenck, O. (2018). “Effect of the soil–pile–structure interaction in seismic analysis: case of liquefiable soils”, *Acta Geotechnica*, 1-17.

[19] Itasca. (2012). *Flac3D: Fast Lagrangian Analysis of Continua in 3 Dimensions, User Manual, Version 5.0*. Itasca Consulting Group Inc., Minneapolis, Minnesota.

[20] Engin, H.K., Septanika, E.G., Brinkgreve, R.B.J. (2008). “Estimation of Pile Group Behavior using Embedded Piles.” In *Proceeding of the 12th International Conference of International Association for Computer Methods and Advances in Geomechanics*, Goa, India, 3231-8.

[21] Oliveira, D.A.F., Wong, P.K. (2011). “Use of Embedded Pile Elements in 3D Modelling of Piled-Raft Foundation.” *Australian Geomechanics Journal,* 46(3).

[22] Tschuchnigg, F., Schweiger, H.F. (2015). “The embedded pile concept – Verification of an efficient tool for modelling complex deep foundations.” *Computers and Geotechnics,* 63, 244-254.

[23] Tradigo, F., Pisanò, F., di Prisco, C. (2016). “On the use of embedded pile elements for the numerical analysis of disconnected piled rafts.” *Computers and Geotechnics,* 72, 89-99.

[24] Bilotta, E., De Sanctis, L., Di Laora, R., D’Onofrio, A., Silvestri, F. (2015). “Importance of seismic site response and soil–structure interaction in dynamic behaviour of a tall building.” *Géotechnique*, 65(5), 391–400.

[25] NTC (2008). Norme Tecniche per le Costruzioni, DM 14/01/2008, GU n.29 del 04/02/2008, Suppl. Ord. 30 (in Italian).

[26] Iervolino, I., Galasso, C., Cosenza, E. (2010). “REXEL: computer aided record selection for code-based seismic structural analysis.” *Bulletin of Earthquake Engineering*, 8(2), 339-362.

[27] Lysmer, J., Kuhlemeyer, R.L. (1969). “Finite Dynamic Model For Infinite Media.” *Journal of the Engineering Mechanics Division*, 95(4), 859-878.

[28] Joyner, W.B., Chen, A.T.F. (1975). "Calculation of nonlinear ground response in earthquakes." *Bulletin of the Seismological Society of America,* 65(5), 1315-1336.

[29] Masing, G. (1926). “Eigenspannungen und verfestigung beim messing.” In *Proceeding of the 2nd International Congress of Applied Mechanics*, Zurich, Switzerland. (in German).

[30] Arroyo, M., Muir Wood, D., Greening, P. D., Medina, L., Rio, J. (2006). “Effects of sample size on bender-based axial G0 measurements.” *Géotechnique*, 56(1), 39-52.

[31] Mánica, M., Ovando, E., Botero, E. (2014). “Assessment of damping models in FLAC.” *Computers and Geotechnics*, 59, 12-20.

[32] Anoyatis, G., Di Laora, R., Mandolini, A., Mylonakis, G. (2013). “Kinematic response of single piles for different boundary conditions: analytical solutions and normalization schemes.” *Soil Dynamics and Earthquake Engineering*, 44, 183-195.

[33] Fan, K., Gazetas, G., Kaynia, A., Kausel, E., Ahmad, S. (1991). “Kinematic seismic response of single piles and pile groups.” *Journal of Geotechnical Engineering*, 117(12), 1860-1879.

[34] Conti, R., Viggiani, G.M.B. (2012). “Evaluation of Soil Dynamic Properties in Centrifuge Tests.” *Journal of Geotechnical and Geoenvironmental Engineering*, 138(7).

[35] CSI (Computers and Structures Inc.). (2004). SAP2000 v10 Integrated Finite Element Analysis and Design of Structures. CSI, Berkeley.

[36] Bouckovalas, G.D., Tsiapas, Y.Z., Theocharis, A.I., Chaloulos, Y.K. (2016). “Ground response at liquefied sites: seismic isolation or amplification?” *Soil Dynamics and Earthquake Engineering*, 91, 329-339.

[37] Conti, R., Morigi, M., Viggiani, G.M.B. (2017). “Filtering effect induced by rigid massless embedded foundations.” *Bulletin of Earthquake Engineering*, 15(3), 1019-1035.

[38] Di Laora, R., Grossi, Y., de Sanctis, L., Viggiani, G.M.B. (2017). “An analytical solution for the rotational component of the Foundation Input Motion induced by a pile group.” *Soil Dynamics and Earthquake Engineering*, 97, 424-438.

[39] Nikolaou, S., Mylonakis, G., Gazetas, G., Tazoh, T. (2001). “Kinematic pile bending during earthquakes: analysis and field measurements.” *Géotechnique*, 51(5), 425-440.

[40] Mylonakis, G., Nikolaou, S., Gazetas, G. (1997). “Soil-Pile-Bridge seismic interaction: kinematic and inertial effects: soft soil.” *Earthquake Engineering & Structural Dynamics*, 26, 337-359.

[41] Di Laora, L., Mylonakis, G., Mandolini, A. (2017). “Size Limitations for Piles in Seismic Regions.” *Earthquake Spectra*, 33(2), 729-756.

TABLES

Table 1. Geotechnical subsoil model: properties of the soil layers

layer	ρ [t/m^3]	V_S [m/s]	v	φ' [°]	c' [kPa]	OCR	K_0
R	1.43	222	0.25	38	2	1.0	0.38
C	1.63	179	0.25	32	25	2.3	0.72
T	1.22	65	0.25	30	2	1.0	0.50
S	1.83	222	0.25	39	2	1.0	0.37
Ps	1.73	273	0.25	40	10	2.3	0.60
Pc	1.63	340	0.25	33	200	3.0	0.83
bedrock	1.83	800	0.25	-	-	1.0	0.50

ρ: mass density; V_S: shear wave velocity; v: Poisson's ratio; φ': friction angle; c': effective cohesion; OCR: over-consolidation ratio; K_0: earth pressure coefficient at rest.

Table 2. Ground motion parameters of the input earthquakes

ID	PGA [g]	PGV [m/s]	PGD [m]	f_d [Hz]	f_m [Hz]	I_a [m/s]	$T_{5\text{-}95}$ [s]	Earthquake location
EQ1	0.192	0.207	0.048	0.88	4.34	0.75	29.8	Montenegro, 15/04/1979
EQ2	0.192	0.070	0.014	6.37	6.23	0.15	7.8	South Iceland, 17/06/2000
EQ3	0.192	0.118	0.039	4.59	4.60	0.53	15.5	Kalamata, 13/10/1997
EQ4	0.192	0.073	0.009	3.84	4.90	0.16	2.7	Off coast of Magion Oros peninsula, 06/08/1983
EQ5	0.192	0.155	0.042	0.56	4.08	0.55	14.2	South Iceland, 17/06/2000
EQ6	0.192	0.073	0.031	7.64	6.15	0.24	19.6	South Iceland, 17/06/2000
EQ7	0.192	0.330	0.102	1.33	2.05	0.55	14.9	Vrancea, 30/08/1986

Table 3. Parameters of the constitutive model adopted for the soil

layer	G_0 [MPa]	v	φ' [°]	c' [kPa]	a	b	x_0
R	70.3	0.25	38	2	1.0	-0.55	-1.1
C	52.3	0.25	32	25	1.0	-0.55	-1.1
T	5.2	0.25	30	2	1.0	-0.5299	-0.0009
S	90.4	0.25	39	2	1.0	-0.6	-1.3
Ps	129.1	0.25	40	10	1.0	-0.6	-1.1
Pc	188.5	0.25	33	200	1.0	-0.6	-1.1
bedrock	1043.8	0.25	-	-	-	-	-

Table 4. Beam elements: geometrical properties

Level	Elevation [m]	section	A_s [m^2]	I_y [m^4]	I_x [m^4]	J_t [m^4]
1	0.00 – 11.55	HE 500B	2.39E-02	1.07E-03	1.26E-04	5.38E-06
2	11.55 – 21.45	HE 400B	1.98E-02	5.77E-04	1.08E-04	3.56E-06
3	21.45 – 31.35	HE 340B	1.71E-02	3.67E-04	9.69E-05	2.57E-06
4	31.35 – 41.25	HE 280B	1.31E-02	1.93E-04	6.60E-05	1.44E-06
5	41.25 – 51.15	HE 240B	1.06E-02	1.13E-04	3.92E-05	1.03E-06
6	51.15 – 61.05	HE 200B	7.81E-03	5.70E-05	2.00E-05	5.93E-07
7	61.05 – 66.00	HE 140B	4.30E-03	1.51E-05	5.50E-06	2.01E-07

Table 5. Shell elements: mechanical, physical and geometrical properties

	E [kPa]	v	ρ [t/m^3]	t_s [m]
shear walls	3.30E+07	0.15	2.50	0.30
core walls	3.30E+07	0.15	2.50	0.25
floor slabs	3.30E+07	0.20	3.11	0.20

Table 6. Foundation solid continuum elements: physical and mechanical properties

	ρ [t/m^3]	G [MPa]	K [MPa]
basement floors	2.50	1.44E+04	1.57E+04
base slab	1.00	1.00E+04	1.10E+04

Table 7. Pile elements: mechanical and geometrical properties of the interfaces

layer	k_s [kN/m^2]	k_n [kN/m^2]	φ_s [°]	φ_n [°]	p [m]
C	1.00E+08	1.00E+08	32	77	6.28
T	1.00E+08	1.00E+08	30	80	6.28
S	1.00E+08	1.00E+08	39	85	6.28
P	1.00E+08	1.00E+08	40	82	6.28
PC	1.00E+08	1.00E+08	33	76	6.28

FIGURES

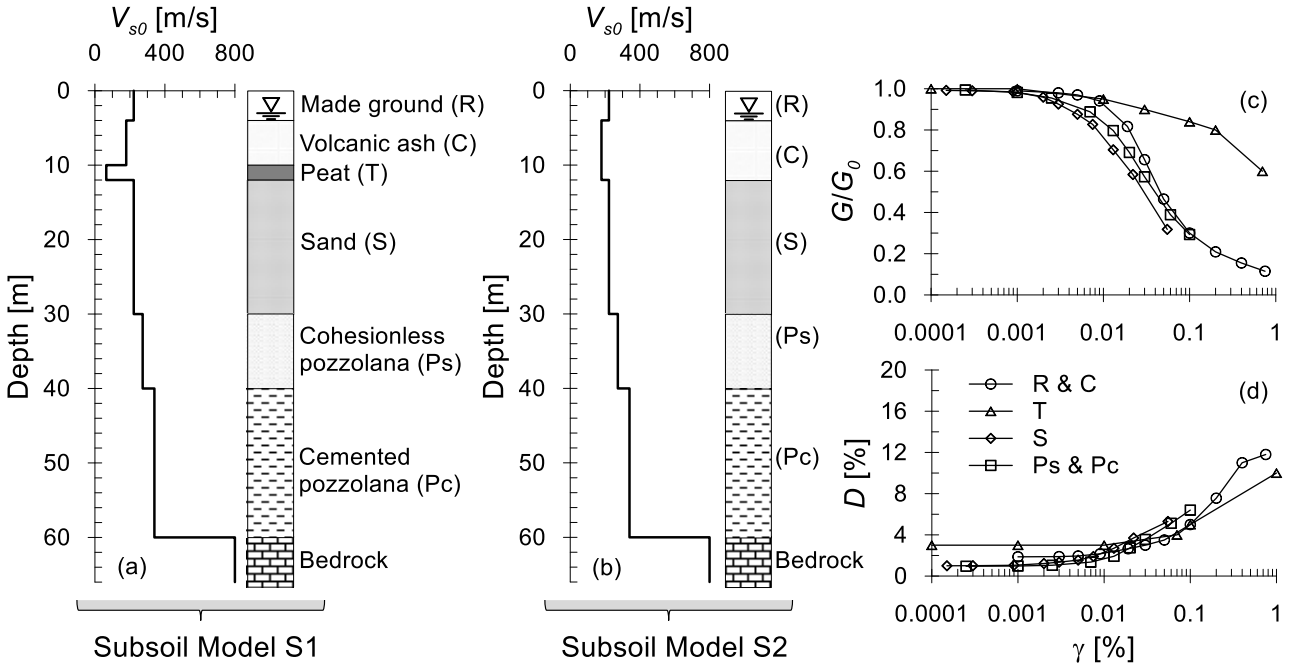

Figure 1. Geotechnical soil models: (a) shear-wave velocity profile and stratigraphic profile for subsoil S1 (with peat layer); (b) shear-wave velocity profile and stratigraphic profile for subsoil S2 (without peat layer); (c) shear modulus reduction curves; (d) damping curves.

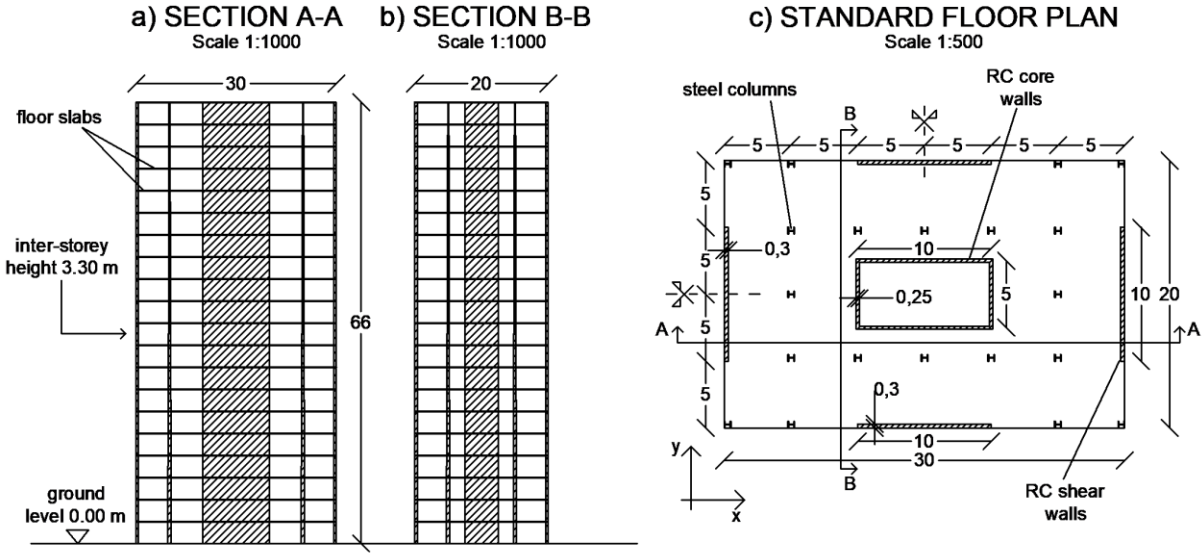

Figure 2. Layout of the structure: (a) section along the x-x direction (direction of the earthquake); (b) section along the y-y direction; (c) standard floor plan.

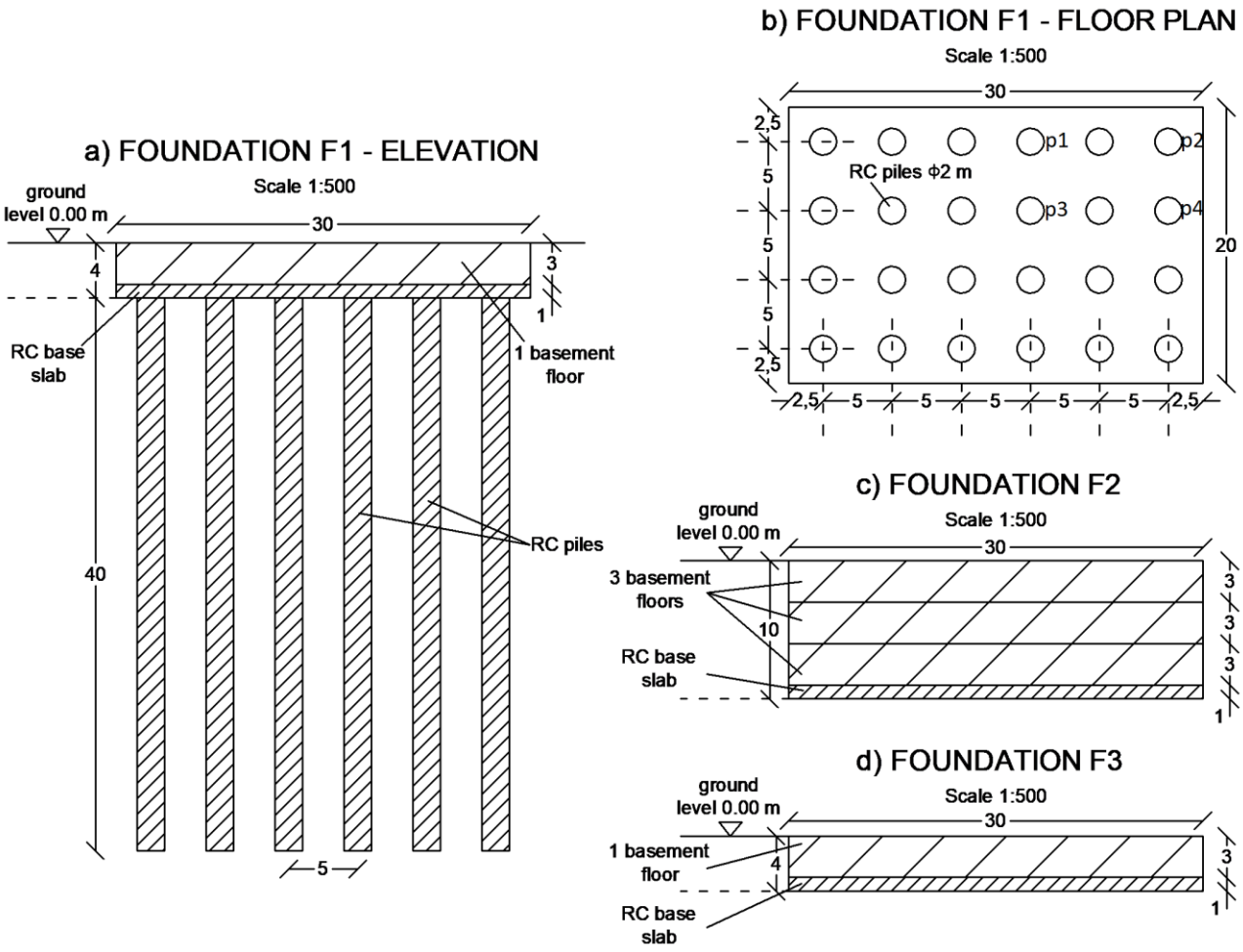

Figure 3. Layout of the foundation systems: (a) elevation and (b) floor plan of the piled-raft foundation – F1; (c) compensated foundation with three basement floors (D= 10 m) – F2; (d) compensated foundation with one basement floors (D= 4 m) – F3.

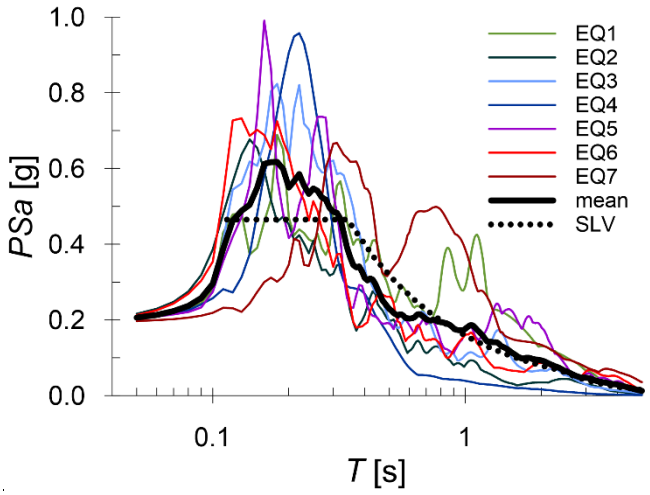

Figure 4. Elastic response spectra at 5% damping of the selected signals, together with their average value and the code-specified spectrum for the life-safety limit state.

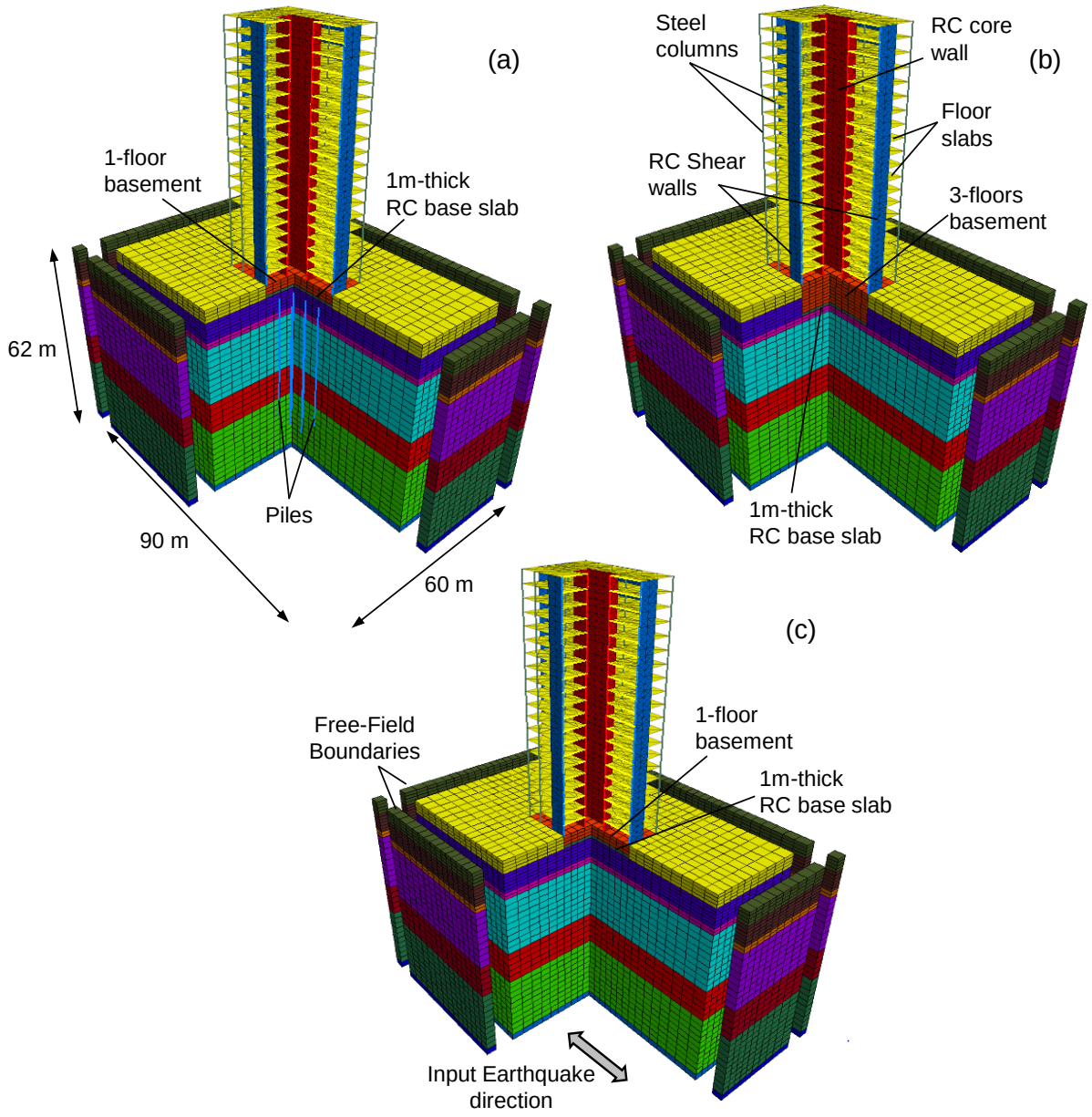

Figure 5. Geometry of the complete soil-foundation-structure numerical models, with foundation systems: (a) F1; (b) F2 and (c) F3.

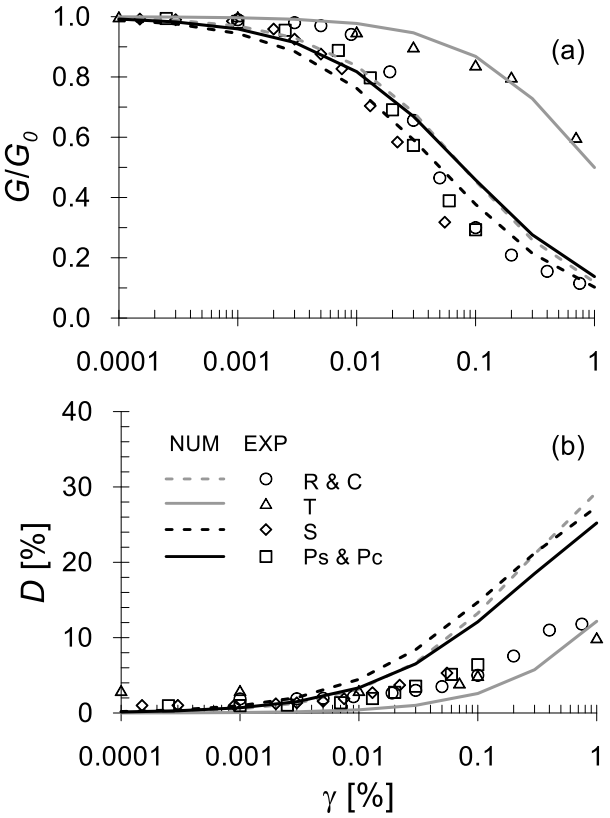

Figure 6. Calibration of the soil constitutive model based on the available experimental data: (a) shear modulus reduction curves; (b) damping curves.

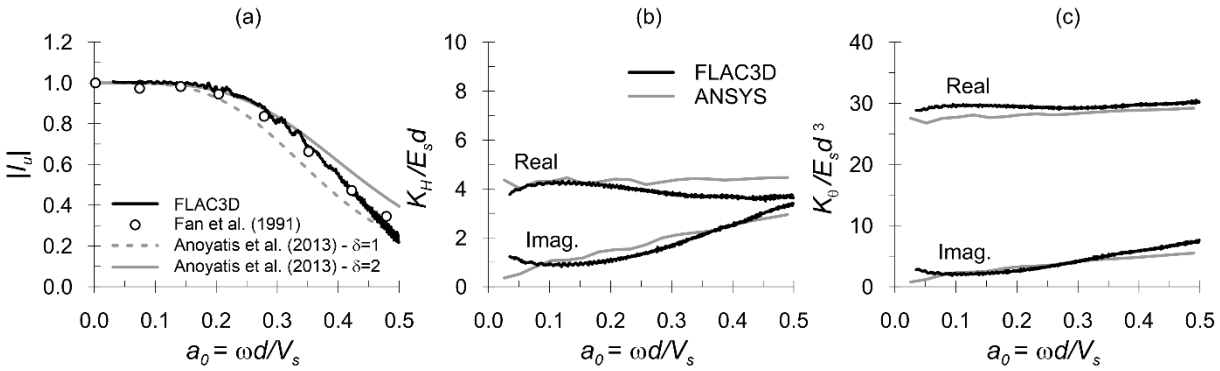

Figure 7. Comparison between the dynamic behaviour of the embedded pile element (FLAC3D) and more rigorous numerical and theoretical solutions, in terms of: (a) kinematic interaction factor I_u; (b) normalized translational impedance function; (c) normalized rocking impedance function.

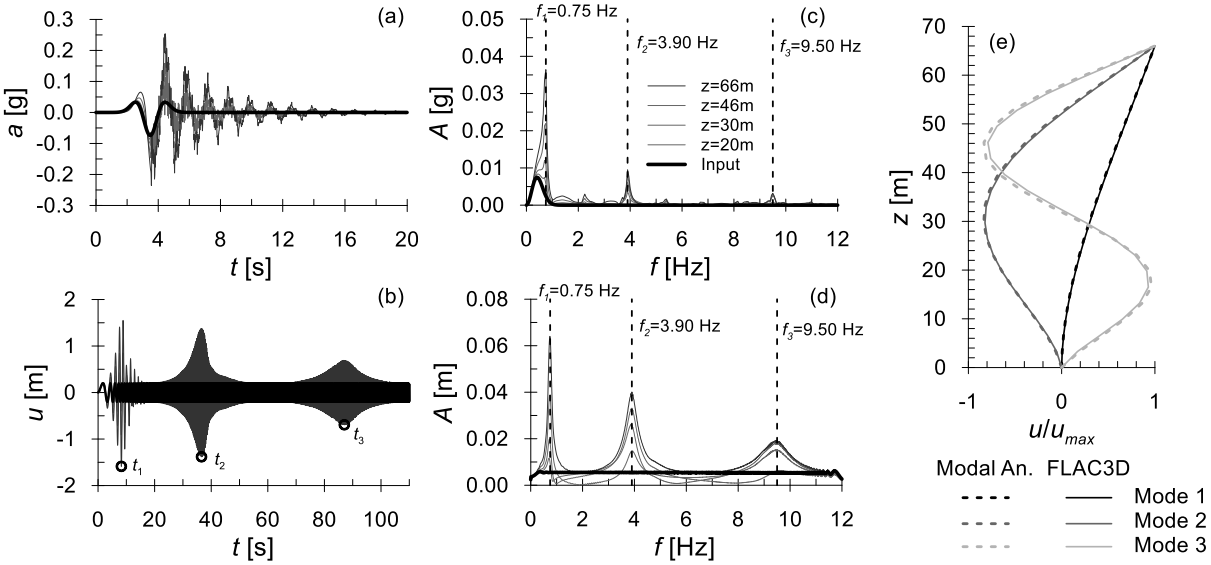

Figure 8. Dynamic identification of the fixed-base structure: (a) acceleration time histories during free vibrations; (b) displacement time histories during forced vibrations; (c) Fourier amplitude spectra of the accelerations during free vibrations; (d) Fourier amplitude spectra of the displacement during forced vibrations; (e) normalised mode shapes for the first three natural frequencies.

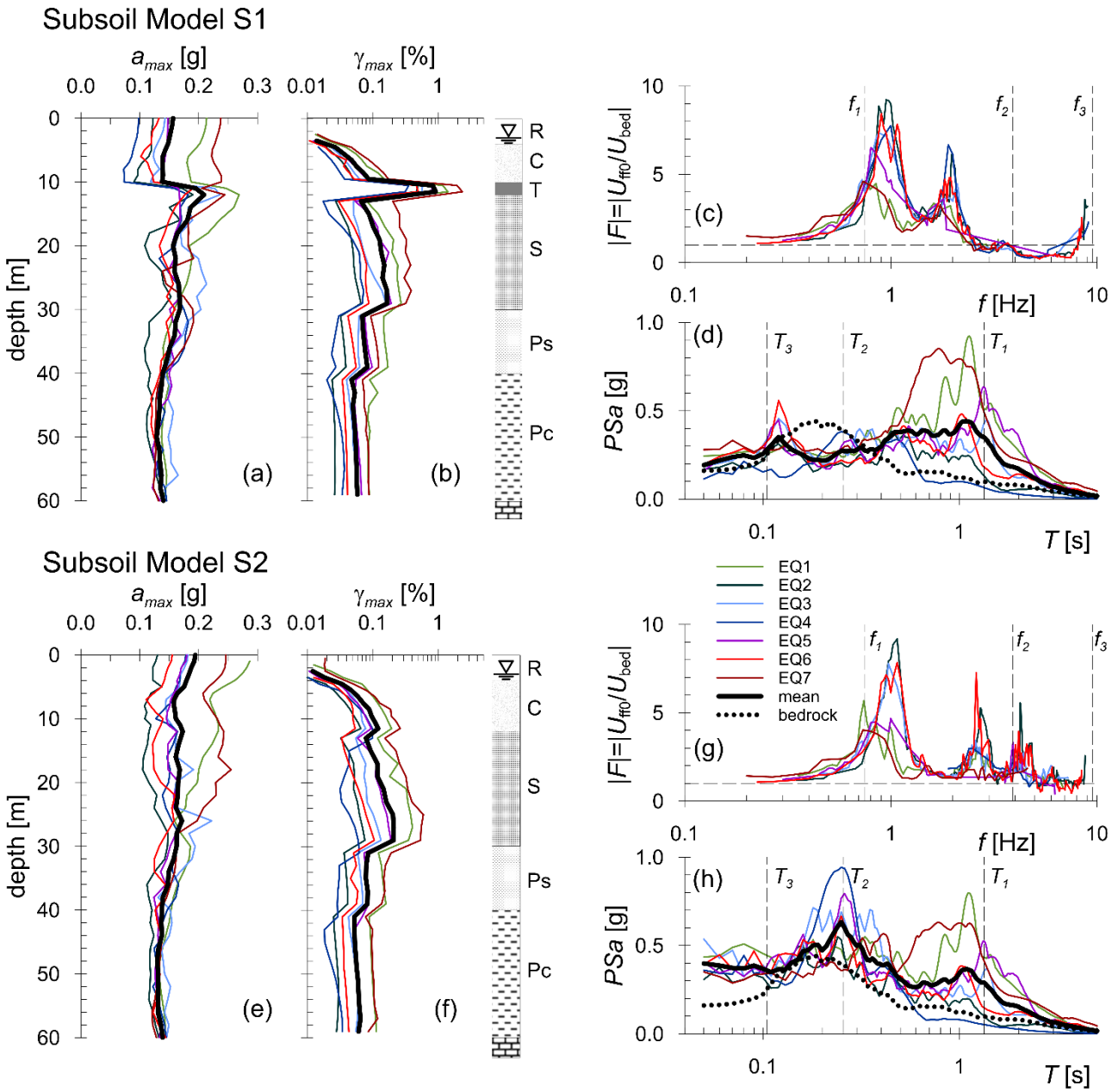

Figure 9. 1D free-field site response analyses. Numerical results obtained for the two subsoil models, S1 and S2, in terms of: profiles of (a, e) maximum acceleration and (b, f) maximum mobilised shear strain; (c, g) surface-to-bedrock amplification functions; (d, h) elastic response spectra at surface.

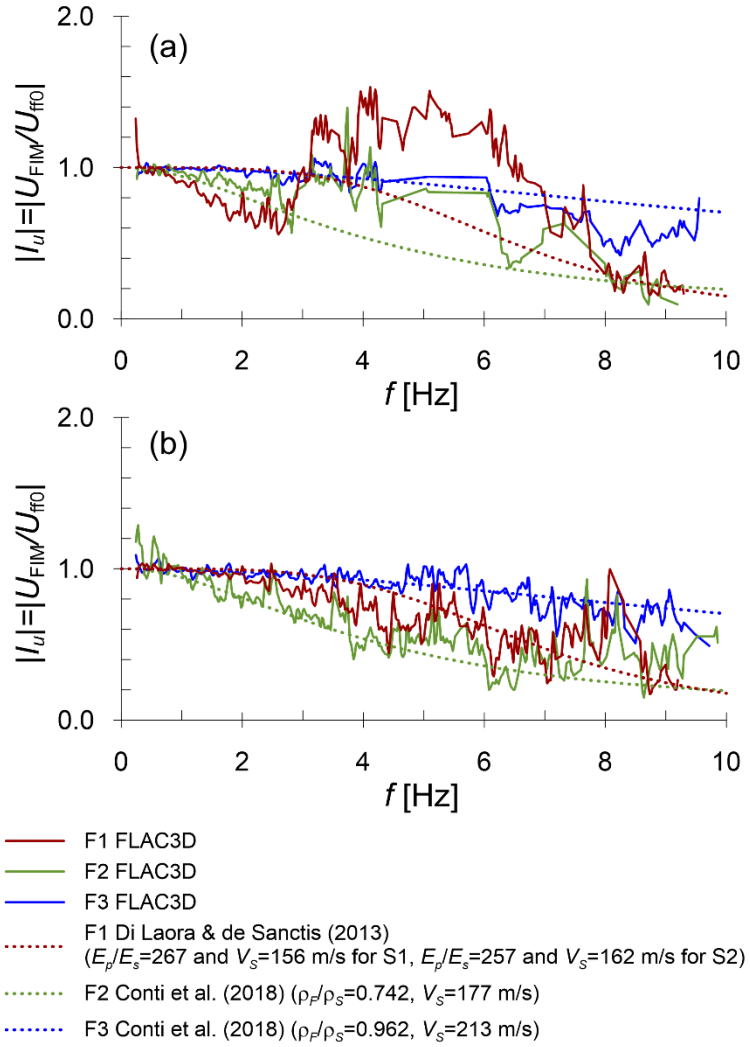

Figure 10. Soil-foundation numerical models. Kinematic interaction factor, $|I_u|$, computed under earthquake EQ2, for the three foundation models: (a) subsoil model S1; (b) subsoil model S2.

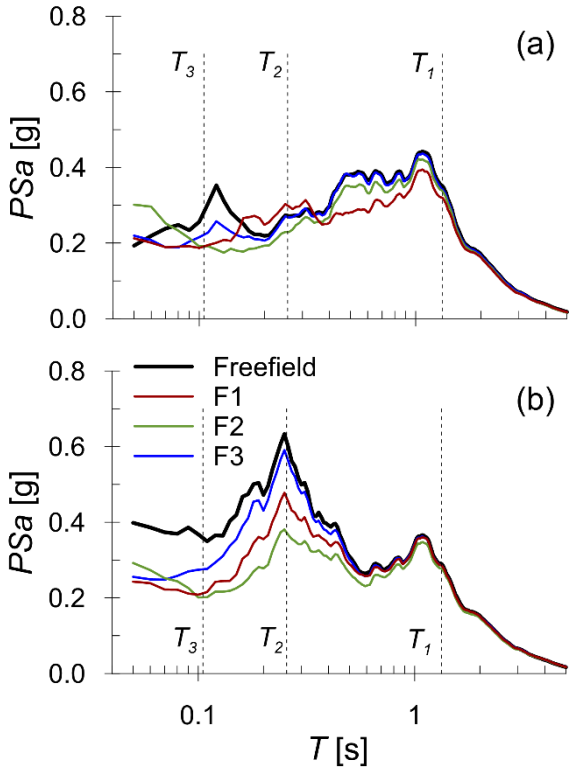

Figure 11. Soil-foundation numerical models. Comparison between the mean values of the 5% damping elastic response spectra of the foundation motion (F1, F2 and F3) and the free field motion: (a) subsoil model S1; (b) subsoil model S2.

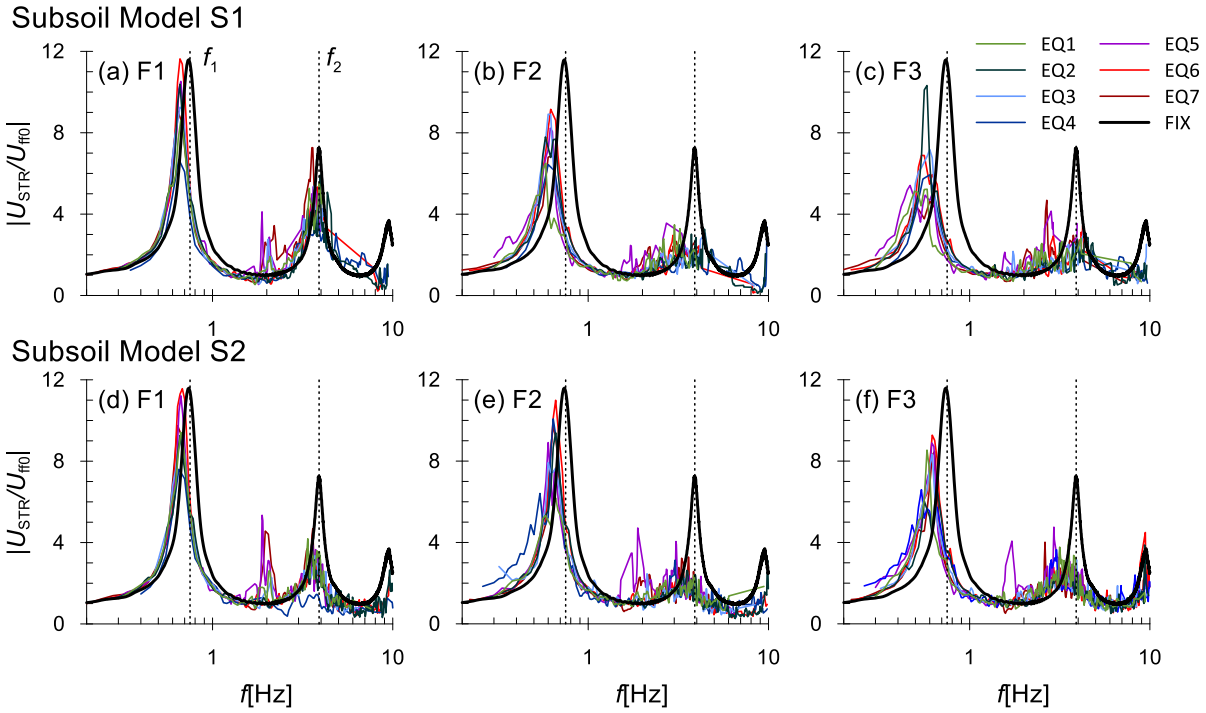

Figure 12. Transfer functions between the displacement of the roof and the free field motion, computed for both the complete soil-foundation-structure numerical models (coloured curves) and the fixed-base model (black curves): (a) foundation model F1 in subsoil S1; (b) foundation model F2 in subsoil S1; (c) foundation model F3 in subsoil S1; (d) foundation model F1 in subsoil S2; (e) foundation model F2 in subsoil S2; (f) foundation model F3 in subsoil S2.

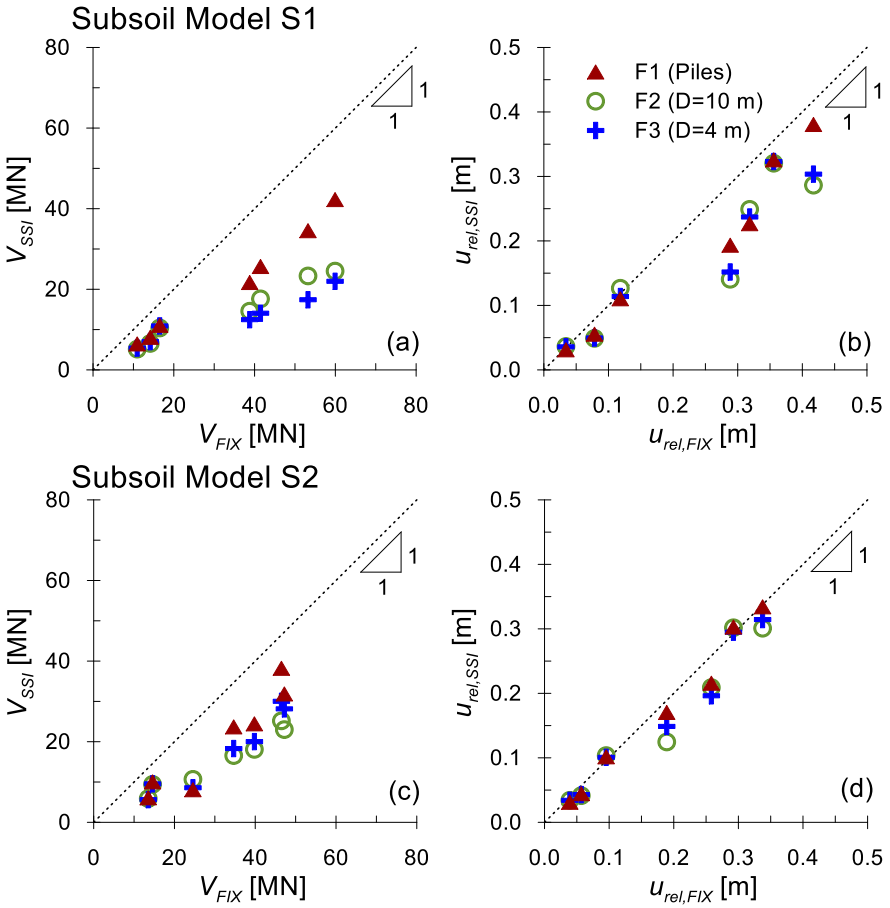

Figure 13. Comparison between the fixed-base model and the complete soil-foundation-structure systems in terms of: (a, c) maximum total shear force at the base; (b, d) maximum relative displacement of the building.

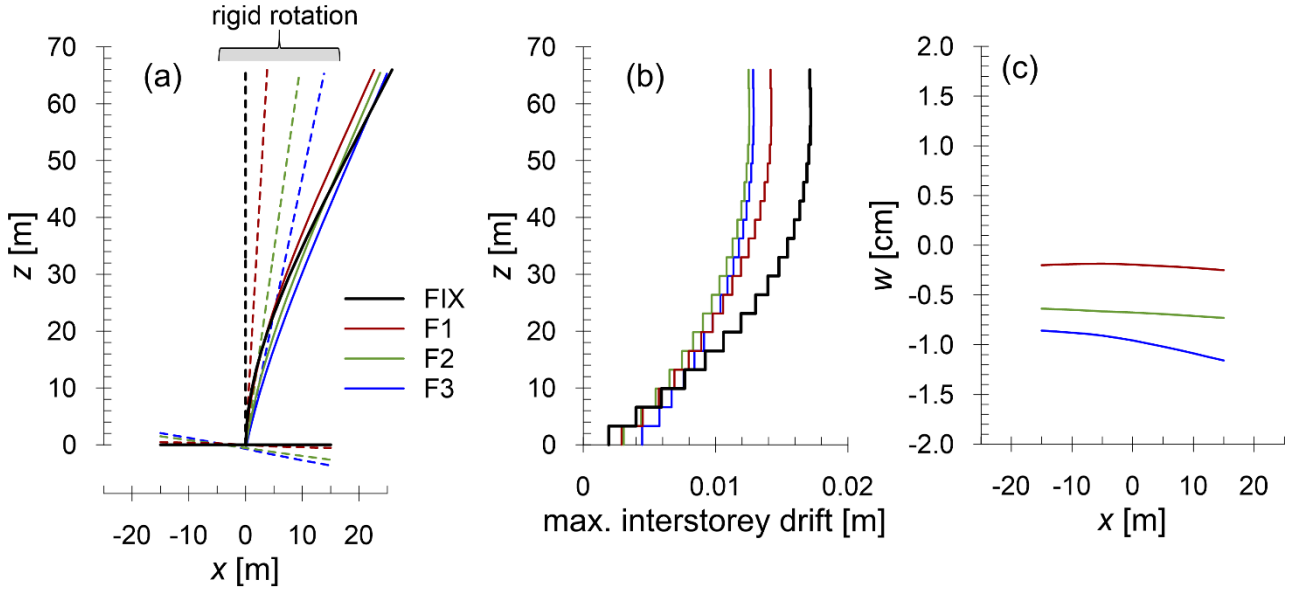

Figure 14. (a) Maximum deformed shape of the structure (deformation factor = 100), (b) maximum drift ratio and (c) residual seismically-induced settlement profiles, computed under the earthquake EQ7 and for the subsoil model S2.

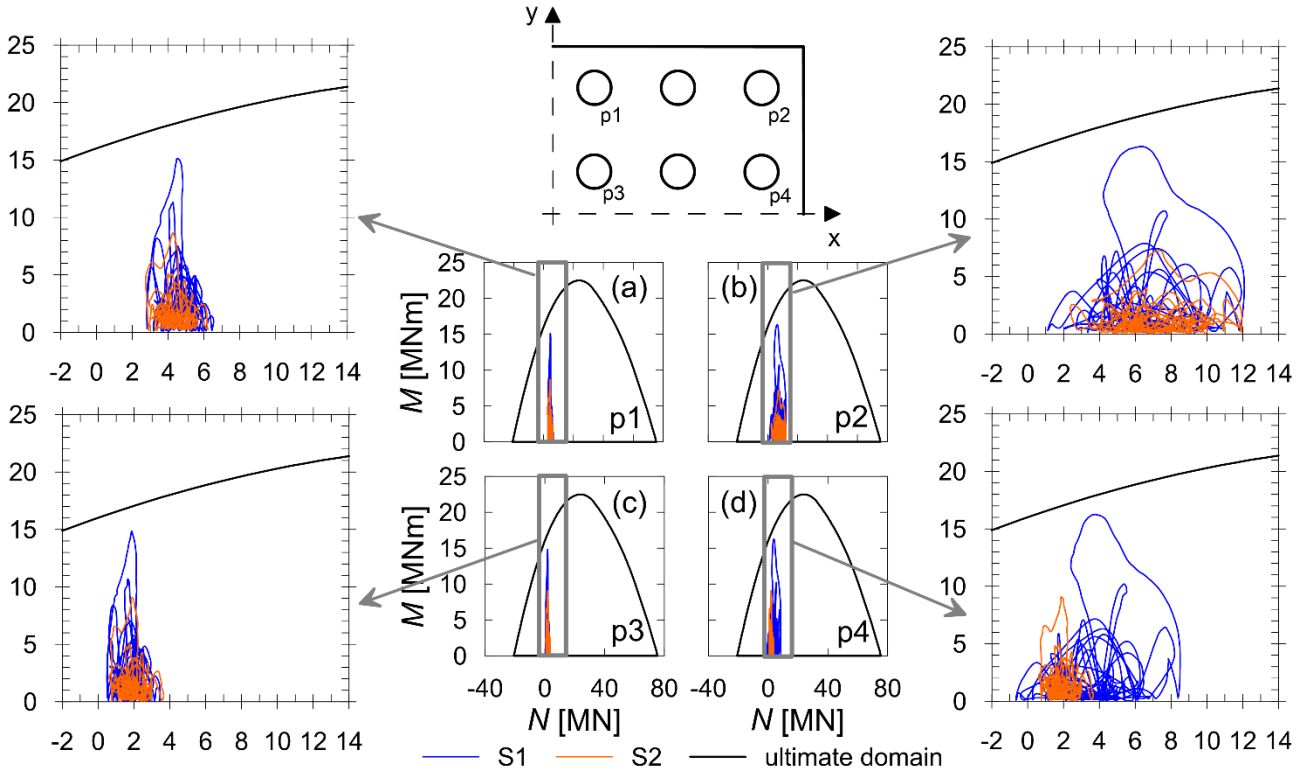

Figure 15. Complete soil-foundation-structure model, earthquake EQ7. Load paths in the N-M space computed at the head section of piles: (a) p1, (b) p2, (c) p3 and (d) p4.

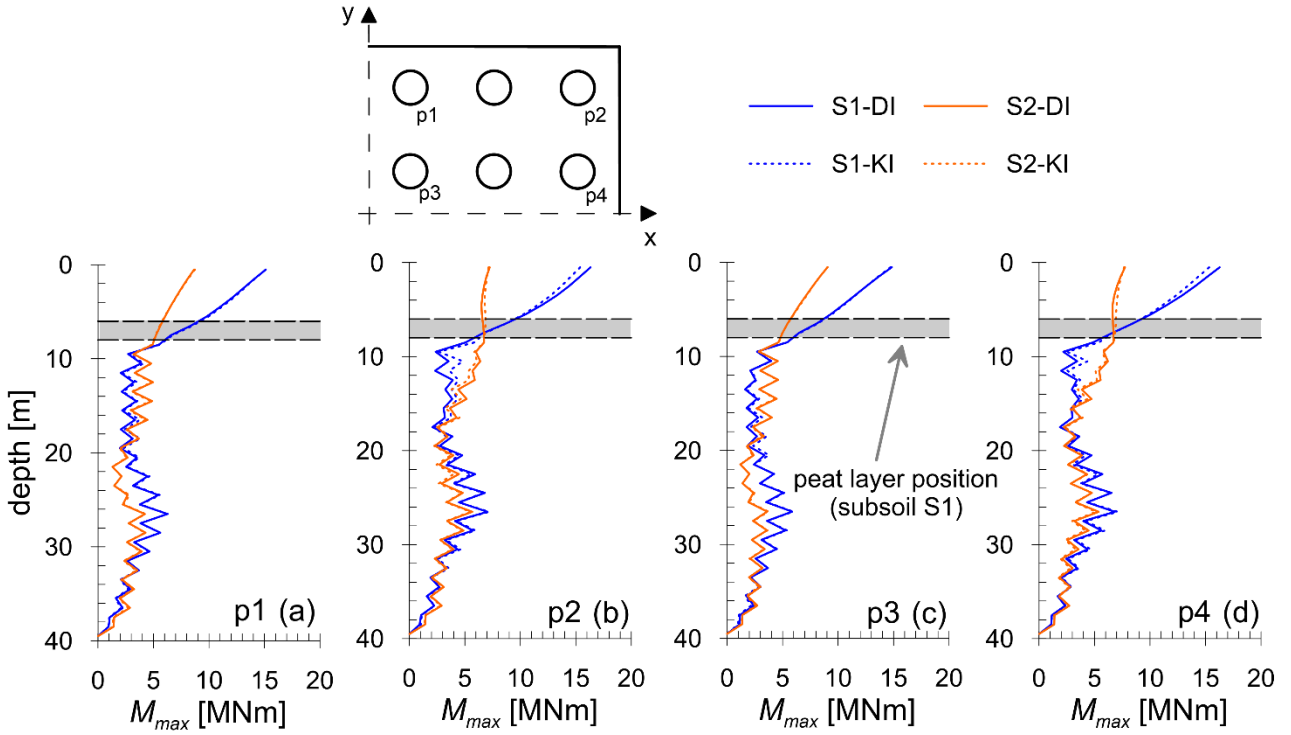

Figure 16. Envelope of the maximum bending moments along piles: (a) p1, (b) p2, (c) p3 and (d) p4, computed during earthquake EQ7.